

Article

Crystallization Behaviors of Anosovite and Silicate Crystals in High CaO and MgO Titanium Slag

Helin Fan ^{1,2}, Dengfu Chen ^{1,2,*}, Tao Liu ^{1,2}, Huamei Duan ^{1,2,*}, Yunwei Huang ^{1,2},
Mujun Long ^{1,2} and Wenjie He ^{1,2}

¹ College of Materials Science and Engineering, Chongqing University, Chongqing 400044, China; fanhelin@cqu.edu.cn (H.F.); cqtao@cqu.edu.cn (T.L.); cqyunwei@cqu.edu.cn (Y.H.); longmujun@cqu.edu.cn (M.L.); hewenjie@cqu.edu.cn (W.H.)

² Chongqing Key Laboratory of Vanadium-Titanium Metallurgy and Advanced Materials, Chongqing University, Chongqing 400044, China

* Correspondence: chendfu@cqu.edu.cn (D.C.); duanhuamei@cqu.edu.cn (H.D.);
Tel.: +86-23-6510-2467 (D.C. & H.D.)

Received: 31 August 2018; Accepted: 21 September 2018; Published: 24 September 2018



Abstract: Electric-furnace smelting has become the dominant process for the production of the titanium slag from ilmenite in China. The crystallization behaviors of anosovite and silicate crystals in the high CaO and MgO titanium slag were studied to insure smooth operation of the smelting process and the efficient separation of titanium slag and metallic iron. The crystallization behaviors were studied by a mathematical model established in this work. Results show that the crystallization order of anosovite and silicate crystals in high CaO and MgO titanium slag during cooling is: $\text{Al}_2\text{TiO}_5 > \text{Ti}_3\text{O}_5 > \text{MgTi}_2\text{O}_5 > \text{MgSiO}_3 > \text{CaSiO}_3 > \text{FeTi}_2\text{O}_5 > \text{Mn}_2\text{SiO}_4 > \text{Fe}_2\text{SiO}_4$. Al_2TiO_5 and Ti_3O_5 have higher crystallization priority and should be responsible for the sharp increase in viscosity of titanium slag during cooling. The total crystallization rates of anosovite and silicate crystals are mainly controlled by Al_2TiO_5 and MgSiO_3 , respectively. The mass ratio of $\text{Ti}_2\text{O}_3/\Sigma\text{TiO}_2$ has a prominent influence on the total crystallization rate of anosovite crystals while the mass ratio of MgO/FeO has a slight influence on the total crystallization rate of anosovite crystals.

Keywords: crystallization behaviors; crystallization rate; anosovite crystals; silicate crystals; titanium slag

1. Introduction

Titanium dioxide and metallic titanium are the main products of titanium metallurgy. Titanium dioxide is widely employed in the fields of coating, painting, paper, plastics, rubber, and ceramic because of its non-toxicity, opacity, whiteness and brightness [1–3]. Metallic titanium has various applications such as aviation, aerospace, biomedical, marine, and nuclear waste storage due to its high corrosion resistance, high specific strength, light weight, high melting point, and high chemical/heat stability [3–5]. A large amount of high-quality titanium-rich materials are increasing required due to the wider and wider application of titanium dioxide and metallic titanium. Titanium-rich materials mainly include two types: Rutile and titanium slag. With the depletion of rutile resource, titanium slag has become the main titanium-rich material to produce the metallic titanium and titanium white in China. The electric-furnace smelting has become the dominant process to produce titanium slag from ilmenite in China. During the process of the electric-furnace smelting, iron oxide in ilmenite concentrate is reduced to metallic iron and titanium oxide in ilmenite is left in the slag (called titanium slag). The flow behavior of titanium slag at high temperature is a crucially significant factor, influencing, for example, the ability to tap the titanium slag from the electric furnace, the efficiency of separation of titanium slag from metal

iron, the foaming extent of titanium slag, and the kinetics of titanium smelting reactions [6]. There is some research about the flow behavior of titanium slag at high temperature in recent decades [7–10]. It has been concluded from the aforementioned research that the titanium slag crystallizes much more easily during tapping from the electric furnace and separation is more difficult from liquid iron than other metallurgical slags. Therefore, the investigation on crystallization behavior of titanium slag at a high temperature will contribute to insuring the smooth operation of the smelting and the efficient separation of titanium slag and metallic iron.

The crystallization of melts consists of two steps: Nucleation and growth [11,12]. The crystallization behavior of melts can be studied by three kinds of methods: Experimental techniques, molecular dynamic simulation, and classical crystallization theory. For example, the crystallization behaviors of mold flux and Ti-bearing blast furnace slag were intensively investigated by the differential scanning calorimeter [13,14], the single hot thermocouple technique/double hot thermocouple technique [15–17], the confocal laser scanning microscope [18–20], and the viscosity-temperature curve method. Watson et al. [21] studied the crystal nucleation and growth in Pd-Ni alloys by the molecular dynamic simulation, which was only suitable for a relatively simple system. Turnbull [22] interpreted convincingly the nucleation phenomena on the basis of the classical crystallization theory. In contrast, there is almost no effective experimental technique to investigate the crystallization behaviors of many different crystals in the relatively complex system of titanium slag. Furthermore, based on the fact that the titanium slag can corrode all refractory oxide containers [9], studies of the crystallization behavior of titanium slag using experiment techniques are extremely difficult and dangerous to carry out. Therefore, few research is focused on the crystallization behavior of titanium slag at a high temperature.

Panzhihua, located in southwestern China, holds ilmenite reserves of 870 million tons, accounting for 35% of total ilmenite reserves in the world [23]. The composition of mineral phases in titanium slag produced from Panzhihua ilmenite is complex due to its high content of CaO and MgO. According to the previous study by Dong et al. [24], the mineral phases in the high CaO and MgO titanium slag consisted of anosovite (FeTi_2O_5 , MgTi_2O_5 , Ti_3O_5 , and Al_2TiO_5), olivine (Fe_2SiO_4 and Mn_2SiO_4), and augite (CaSiO_3 and MgSiO_3) as determined by X-ray diffraction and Energy Dispersive Spectrometer. Fan et al. [25] also confirmed the complex composition of mineral phases in the high CaO and MgO titanium slag. Therefore, the crystallization behaviors of crystals in the high CaO and MgO titanium slag would become more complex.

In this work, a mathematical model was established to describe the crystallization behaviors of anosovite and silicate crystals in the high CaO and MgO titanium slag. Specifically, two main issues will be addressed. First, the crystallization behaviors of anosovite and silicate crystals in the high CaO and MgO titanium slag will be determined. The crystallization ability, crystallization order, and optimum temperature ranges of different crystals in the high CaO and MgO titanium slag will be analyzed and discussed in detail. Second, the effect of the composition of titanium slag on the crystallization behaviors of anosovite crystals will be investigated. Based on the results, the smelting parameters of titanium slag will be adjusted in industrial production in further works to enhance the smooth operation of the electric furnace and to improve the separation of titanium slag and metallic iron.

2. Mathematical Model

According to the classical crystallization kinetics from D. Turnbull et al. [26], the nucleation rate I of a crystal and the formation energy of a crystal nucleus could be expressed as Equations (1) and (2) respectively.

$$I = \frac{nD}{a_0^2} \exp\left(-\frac{\Delta G^*}{kT}\right) \quad (1)$$

$$\Delta G^* = \frac{16\pi\sigma^3}{3(\Delta g_V)^2} \quad (2)$$

$$n = \frac{1}{a_0^3} \quad (3)$$

where I is the nucleation rate of a crystal in $\text{m}^{-3} \cdot \text{s}^{-1}$, n is the atom number per unit volume, D is the self-diffusion coefficient of atoms in the melt in $\text{m}^2 \cdot \text{s}^{-1}$, a_0 is the lattice parameter in m, ΔG^* is the formation energy of crystal nucleus in $\text{J} \cdot \text{mol}^{-1}$, k is the Boltzmann constant, T is the temperature of the melt in K, π is the pi constant, σ is the interfacial energy between the melt and crystal in $\text{J} \cdot \text{m}^{-2}$, and Δg_V is the change of Gibbs free energy per unit volume in $\text{J} \cdot \text{mol}^{-1} \cdot \text{m}^{-3}$.

The relationship between the self-diffusion coefficient D and the viscosity η could be expressed as Equation (4) [27,28].

$$D = \frac{kT}{3\pi a_0 \eta} \quad (4)$$

$$\Delta g_V = \frac{\Delta H_m^g}{V} \Delta T_r \quad (5)$$

where η is the viscosity of the melt in $\text{Pa} \cdot \text{s}$, ΔH_m^g is the fusion heat per mole melt in $\text{J} \cdot \text{mol}^{-1}$, V is the mole volume of the crystal in $\text{m}^3 \cdot \text{mole}^{-1}$, and $\Delta T_r = 1 - T_r$ ($T_r = T/T_m$, T_m is the melting temperature of a crystal in K).

The viscosity involves the physicochemical property of the melt and can be estimated by the National Physical Laboratory model [29]. The optical basicity of the slag component for the calculation of titanium slag is from references [29–31]. The relationship between the viscosity and temperature was expressed as Equation (6).

$$\ln \eta = \ln A + B/T \quad (6)$$

The relationship between optical basicity and constants A and B could be expressed as Equations (7) and (8) [29].

$$\ln \frac{B}{1000} = -1.77 + \frac{2.88}{\Lambda} \quad (7)$$

$$\ln A = -232.69(\Lambda)^2 + 357.32\Lambda - 144.17 \quad (8)$$

The optical basicity of the titanium slag could be calculated by the following Equation (9).

$$\Lambda = \frac{\sum \chi_i n_i \Lambda_i}{\sum \chi_i n_i} \quad (9)$$

where χ_i and n_i is the mole fraction and the number of oxygen atoms of an independent component respectively and Λ_i is the optical basicity of the corresponding independent component.

Taking Equations (2)–(5) into Equation (1), the nucleation rate I of a crystal can be deduced as Equation (10).

$$I = \frac{kT}{3\pi a_0^6 \eta} \exp \left\{ -\frac{16\pi}{3T_r(\Delta T_r)^2} \left[\frac{(N_0 V^2)^{1/3} \sigma}{\Delta H_m^g} \right]^3 \left(\frac{\Delta H_m^g}{RT_m} \right) \right\} \quad (10)$$

where α and β are the two dimensionless parameters which have the important influence on the crystal melting process. α and β could be expressed as following Equations (11) and (12) [32].

$$\alpha = \frac{(N_0 V^2)^{1/3} \sigma}{\Delta H_m^g} \quad (11)$$

$$\beta = \frac{\Delta H_m^g}{RT_m} \quad (12)$$

where N_0 is the Avogadro constant.

Combined with Equations (11) and (12), the nucleation rate I of a crystal could be expressed as Equation (13).

$$I = \frac{kT}{3\pi a_0^6 \eta} \exp \left[-\frac{16\pi\alpha^3\beta}{3T_r(\Delta T_r)^2} \right] \quad (13)$$

According to the classical kinetics of crystallization, the growth rate I_L of a crystal could be expressed as Equation (14).

$$I_L = \frac{f_s D}{a_0} \left[1 - \exp \left(\frac{\Delta G_g}{RT} \right) \right] \quad (14)$$

where f_s is the proportionality coefficient of the position benefiting the atomic adsorption on the crystal at interface between melt and crystal and ΔG_g is the change of Gibbs free energy per mole between the melt and crystal. f_s and ΔG_g could be expressed as Equations (15) and (16) [33].

$$f_s = \begin{cases} 1 & \Delta H_m 2RT_m \\ 0.2 \frac{T_m - T}{T_m} & \Delta H_m 4RT_m \end{cases} \quad (15)$$

$$\Delta G_g = \Delta H_m^s \frac{T_m - T}{T_m} \quad (16)$$

Combined with Equations (14)–(16), the growth rate of a crystal could be expressed as Equation (17).

$$I_L = \frac{f_s kT}{3\pi a_0^2 \eta} \left\{ 1 - \exp \left[\left(\frac{\Delta H_m^s}{RT_m} \right) \left(\frac{\Delta T_r}{T_r} \right) \right] \right\} \quad (17)$$

Combined with Equations (11), (12) and (17), the growth rate of a crystal could be expressed as Equation (18) [34].

$$I_L = \frac{f_s kT}{3\pi a_0^2 \eta} \left[1 - \exp \left(-\beta \frac{\Delta T}{T_r} \right) \right] \quad (18)$$

According to a previous research by Uhlmann et al. [33], the volume fraction (x) of a crystal could be expressed as a function with the nucleation rate (I), growth rate (I_L) and time t .

$$x = \frac{1}{3} \pi I I_L^3 t^4 \quad (19)$$

$$r_i = \frac{1}{3} \pi I I_L^3 \quad (20)$$

The total crystallization rate of a crystal r_{total} could be expressed as a function with mole fraction (ω_i) and crystallization rate (r_i) of a given crystal as Equation (21).

$$r_{total} = \sum_i \omega_i r_i \quad (21)$$

The chemical composition of titanium slag is as follows (wt. %): $\text{TiO}_2 = 55.20$, $\text{FeO} = 12.21$, $\text{SiO}_2 = 5.89$, $\text{MnO} = 1.53$, $\text{MgO} = 2.51$, $\text{Al}_2\text{O}_3 = 2.83$, $\text{CaO} = 1.00$, and $\text{Ti}_2\text{O}_3 = 18.92$. The structural parameters and melting temperatures of these crystals in titanium slag are listed in Table 1 [35–37]. $a_0 = (a \times b \times c)^{1/3}$, in which a , b and c are lattice parameters of crystals in the titanium slag. Because the content of Mn-anosovite is small, Mn-anosovite is neglected in this work.

Table 1. Structural parameters and melting temperature of crystals in titanium slag.

Mineral Phase	Chemical Formula	a_0 (Å)	T_m (K)
Anosovite	FeTi ₂ O ₅	7.192 [35]	1767 [36]
	MgTi ₂ O ₅	7.145 [35]	1930 [37]
	Ti ₃ O ₅	7.186 [35]	1991 [37]
	Al ₂ TiO ₅	6.858 [35]	2133 [36]
Olivine	Fe ₂ SiO ₄	6.752 [35]	1478 [36]
	Mn ₂ SiO ₄	6.878 [35]	1618 [36]
Augite	CaSiO ₃	7.351 [35]	1817 [36]
	MgSiO ₃	7.464 [35]	1830 [36]

3. Results and Discussion

3.1. Nucleation and Growth of Crystals in Titanium Slag

3.1.1. Nucleation and Growth of Anosovite Crystals

From the viewpoint of the classical crystallization theory, the crystallization process includes two stages: Nucleation and growth. The nucleation refers to the generation of a crystal nucleus from a mother phase. The growth of the crystal is realized by the growth of the crystal nucleus. Although the nucleation process is transitory compared with the subsequent growth process, the nucleation is completely different from the growth process.

Figure 1 displays the nucleation and growth rates of different anosovite crystals in the titanium slag. It can be observed from Figure 1 that the nucleation rates first increase from zero to the maximum value and then decrease to zero with the degree of undercooling increasing from zero. The profiles of nucleation rates should be attributed to the interaction of two contradictory factors related to the crystallization process: The degree of undercooling and diffusion ability of atoms. With a too high or too low degree of undercooling, the small nucleation rates of crystals are formed. With a reasonable degree of undercooling, the maximum nucleation rates of crystals are formed. The profiles of growth rates have the similar characteristics to the profiles of nucleation rates. The maximum nucleation rates and maximum growth rates of anosovite crystals follow the same order: Al₂TiO₅ > Ti₃O₅ > MgTi₂O₅ > FeTi₂O₅. The maximum nucleation rates (maximum growth rates) of different anosovite crystals are very different, indicating that the crystallization abilities of different anosovite crystals may differ remarkably.

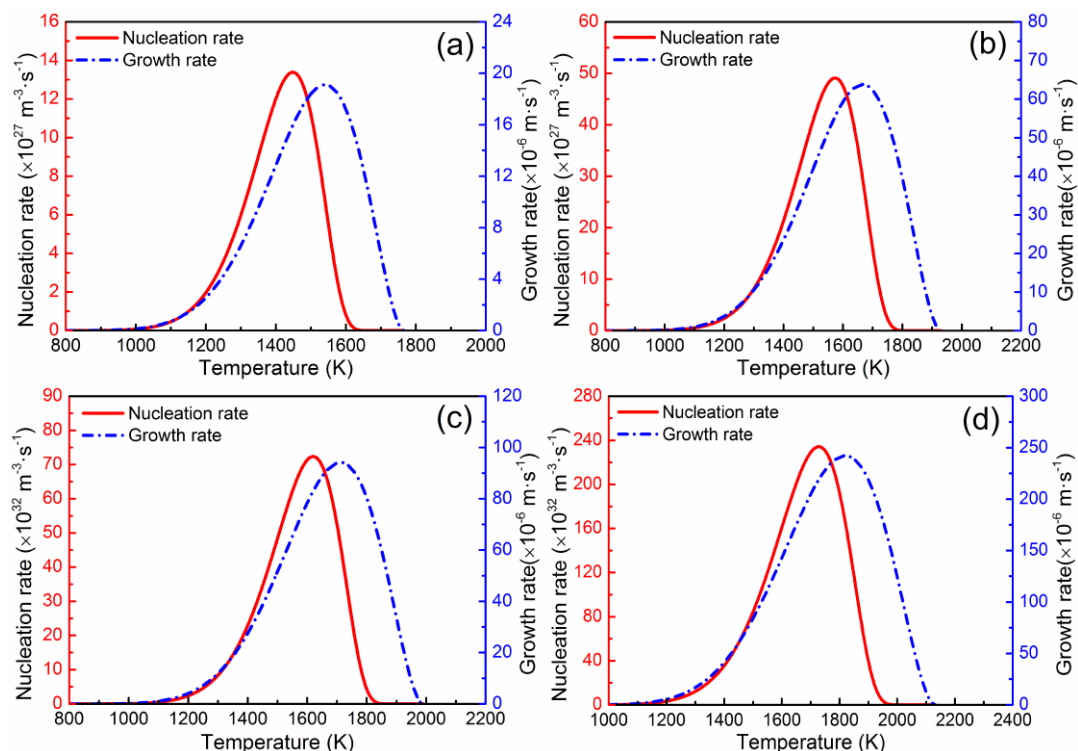


Figure 1. Nucleation and growth rates of different anosovite crystals: (a) FeTi_2O_5 , (b) MgTi_2O_5 , (c) Ti_3O_5 , and (d) Al_2TiO_5 .

3.1.2. Nucleation and Growth of Silicate Crystals

Figure 2 displays the nucleation and growth rates of different silicate crystals in titanium slag. It can be observed from Figure 2 that the profiles of nucleation rates of silicate crystals have the similar characteristics to the profiles of nucleation rates of anosovite crystals. The profiles of growth rates of silicate crystals have the similar characteristics to the profiles of growth rates of anosovite crystals. Both the maximum nucleation rates and the maximum growth rates of silicate crystals follow the same order: $\text{MgSiO}_3 > \text{CaSiO}_3 > \text{Mn}_2\text{SiO}_4 > \text{Fe}_2\text{SiO}_4$. The maximum nucleation rates (maximum growth rates) of different silicate crystals are similar in value, indicating that silicate crystals have the similar crystallization ability. The maximum nucleation rates (maximum growth rates) of silicate crystals are much smaller than those of anosovite crystals, demonstrating that silicate crystals may have much a weaker crystallization ability than the anosovite crystals.

The driving force of the crystallization and diffusion ability of atoms is large enough when the temperature is between that of the maximum nucleation rate and the maximum growth rate. Therefore, the range from the temperature of maximum nucleation rate to the temperature of maximum growth rate is specified as the characteristic temperature range of crystallization in this work. It is easy to nucleate, grow and obtain coarse grain within the characteristic temperature range. Figure 3 displays the characteristic temperature ranges of crystallization of anosovite and silicate crystals in titanium slag. It can be observed from Figure 3 that the characteristic temperature ranges of crystallization of crystals in titanium slag follow the sequence of $\text{Al}_2\text{TiO}_5 > \text{Ti}_3\text{O}_5 > \text{MgTi}_2\text{O}_5 > \text{MgSiO}_3 > \text{CaSiO}_3 > \text{FeTi}_2\text{O}_5 > \text{Mn}_2\text{SiO}_4 > \text{Fe}_2\text{SiO}_4$. The characteristic temperature ranges of crystallization of these crystals are in sequence as follows: 1728–1819 K, 1620–1712 K, 1573–1666 K, 1497–1589 K, 1487–1579 K, 1448–1540 K, 1333–1424 K, 1225–1312 K. The characteristic temperature ranges are consistent with the tapping temperature of smelting ilmenite to titanium slag in an electric furnace.

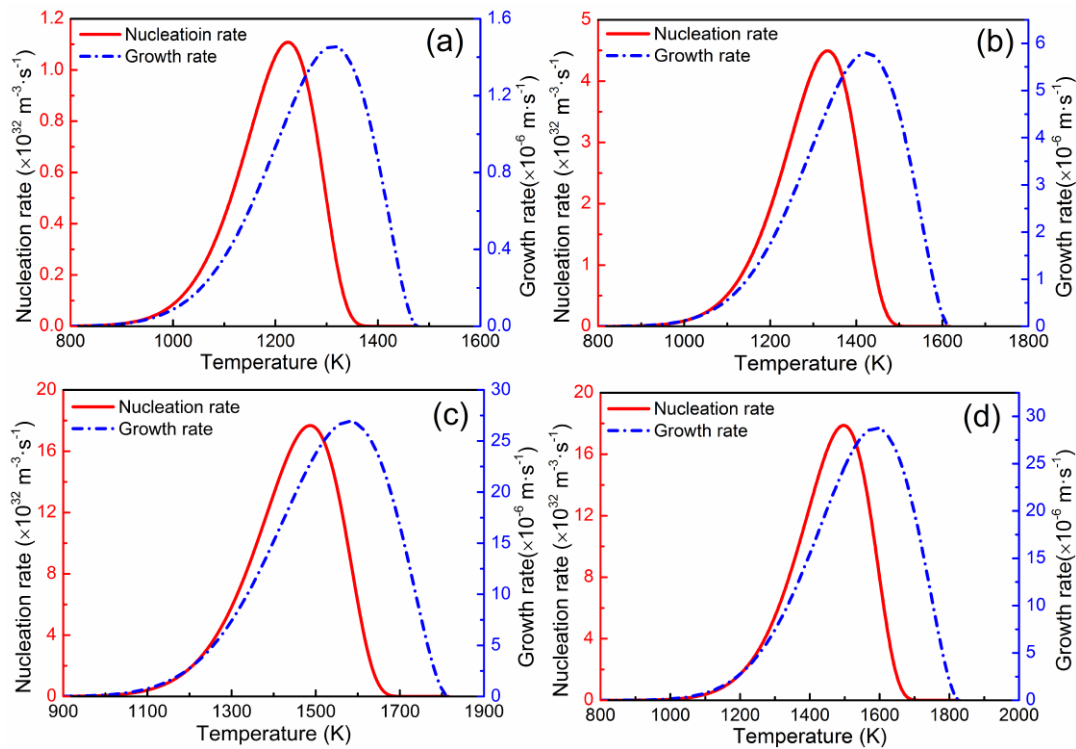


Figure 2. Nucleation and growth rates of different silicate crystals: (a) Fe_2SiO_4 , (b) Mn_2SiO_4 , (c) CaSiO_3 and (d) MgSiO_3 .

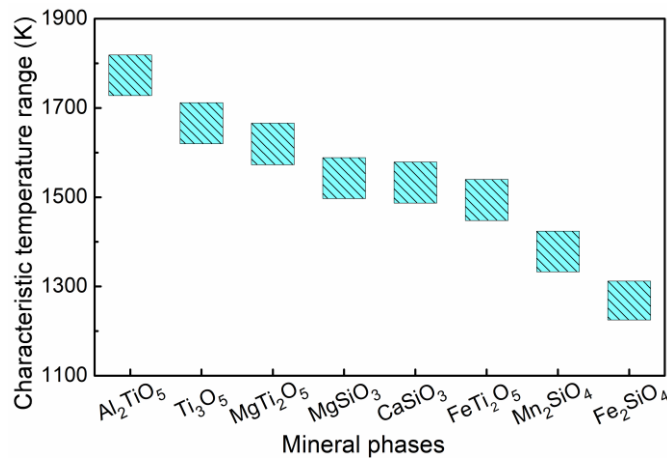


Figure 3. Characteristic temperature ranges for crystallization of anosovite and silicate crystals in titanium slag.

3.2. Crystallization Behavior of Anosovite and Silicate Crystals

The crystallization rate of crystals is the main and direct indicator for evaluating the crystallization behavior. Therefore, the optimum temperature range of crystallization can be determined by the crystallization rate of crystals. Figure 4 shows the crystallization rates of different anosovite and silicate crystals in titanium slag. It can be seen from Figure 4a that the maximum crystallization rate of Al_2TiO_5 has two higher orders of magnitude than Ti_3O_5 . The maximum crystallization rate of MgTi_2O_5 has five higher orders of magnitude than FeTi_2O_5 . It is notable that the total crystallization rate of anosovite crystals is mainly controlled by Al_2TiO_5 . The optimum temperature ranges of anosovite crystals are as the following: Al_2TiO_5 (1744–1804 K) > Ti_3O_5 (1636–1696 K) > MgTi_2O_5 (1589–1649 K) > FeTi_2O_5 (1346–1406 K). It can be seen from Figure 4b that the maximum crystallization rates of

MgSiO₃ and CaSiO₃ have three higher orders of magnitude than Mn₂SiO₄ and five higher orders of magnitude Fe₂SiO₄. The total crystallization rate of silicate crystals is mainly controlled by MgSiO₃. The optimum temperature ranges of silicate crystals are as the following: MgSiO₃ (1512–1572K) > CaSiO₃ (1502–1562 K) > Mn₂SiO₄ (1346–1406 K) > Fe₂SiO₄ (1236–1296 K).

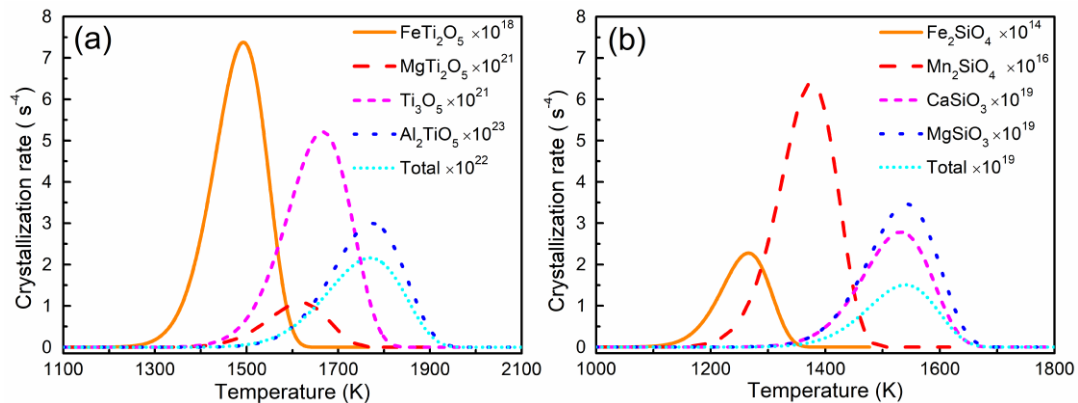


Figure 4. Crystallization rate of different crystals in titanium slag: (a) anosovite and (b) silicate.

Notably, both the maximum crystallization rate and the optimum temperature ranges of Al₂TiO₅ and Ti₃O₅ are much higher than other crystals in high CaO and MgO titanium slag. The crystallization priority of Al₂TiO₅ and Ti₃O₅ is consistent with the report from Zhao et al. [7] that the sharp increase in viscosity of titanium slag may be caused by the high Al₂O₃ and Ti₂O₃ content in titanium slag. The accuracy of the mathematical model can be preliminarily demonstrated by the consistency between the crystallization priority of Al₂TiO₅ and Ti₃O₅ in titanium slag and the remarkable effect of Al₂O₃ and Ti₃O₅ on viscosity of titanium slag. This result implies that the variation of Al₂O₃ and Ti₃O₅ content in titanium slag should be paid close attention to during the electric-furnace smelting process. Furthermore, Song et al. [38] and Handfield et al. [9] reported that the melting temperature of the titanium slag, whose composition was similar with the titanium slag in this work, was approximately 1873 K. Al₂TiO₅ in this work has the crystallization rate of 1.03×10^{23} (s⁻⁴) at the temperature of 1873 K. The accuracy of the mathematical model can be further demonstrated by the crystallization rate of Al₂TiO₅ at the melting temperature of 1873 K.

T_c is the peak temperature of maximum crystallization rate of crystals. T_m is the melting point of the crystal. $(T_m - T_c)/T_m$ represents the crystallization process during cooling. Figure 5a shows the relationship between melting temperature and the crystallization process. It can be seen from Figure 5a that the crystal with higher melting temperature crystallizes earlier during cooling. This crystallization order agrees with the work from Diao et al. [39] that the mineral phases of vanadium-chromium slag crystallized in the order of their melt points during cooling. Figure 5b shows the relationship between the maximum crystallization rate and the peak temperature. It can be seen from Figure 5b that the crystallization order of crystals in titanium slag is obtained during cooling as follows: Al₂TiO₅ > Ti₃O₅ > MgTi₂O₅ > MgSiO₃ > CaSiO₃ > FeTi₂O₅ > Mn₂SiO₄ > Fe₂SiO₄. The crystal with a higher maximum crystallization rate has a higher peak temperature. This relationship may be ascribed to the strong diffusion ability of atoms with the higher temperature. Obviously, anosovite crystals crystallize overall earlier than silicate crystals during cooling. The crystallization order in this work is consistent with the reports from Pistorius et al. [40] and Wang et al. [41] that anosovite and silicate crystals occupied the center and outer layer of titanium slag particle, respectively. The accuracy of the mathematical model can be demonstrated once again by the consistency between the overall crystallization order and spatial distribution of anosovite and silicate crystals in high CaO and MgO titanium slag.

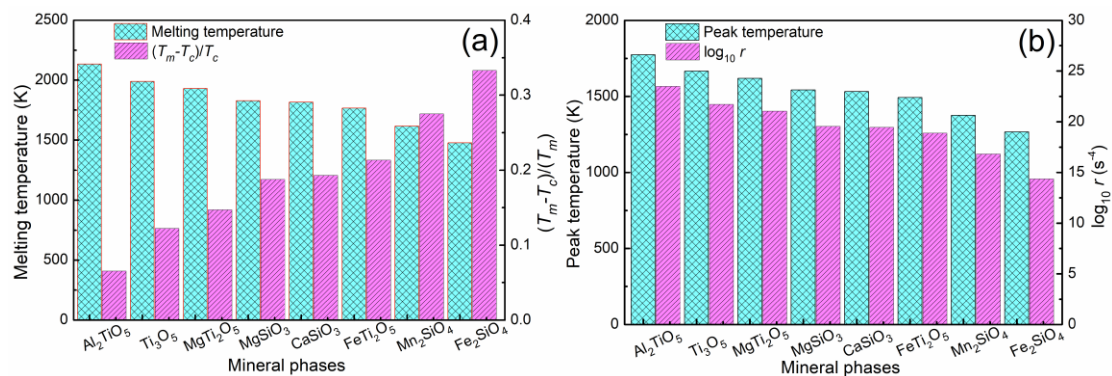


Figure 5. (a) Relationship between melting temperature and $(T_m - T_c)/T_c$ and (b) Relationship between maximum crystallization rate and peak temperature.

3.3. Effects of Slag Composition on Crystallization Behaviors of Anosovite Crystals

To investigate effects of the slag composition on crystallization behaviors of anosovite crystals, the mass ratio of $\text{Ti}_2\text{O}_3/\Sigma\text{TiO}_2$ and the mass ratio of MgO/FeO are selected as two variables. The chemical compositions of slag are shown in Table 2. The mass ratio of $\text{Ti}_2\text{O}_3/\Sigma\text{TiO}_2$ is from 0.05 (CS1) to 0.45 (CS5) and the mass ratio of MgO/FeO is from 0.10 (CS6) to 0.90 (CS10).

Table 2. Compositions of titanium slag (wt. %).

Samples	TiO ₂	FeO	SiO ₂	MnO	MgO	Al ₂ O ₃	CaO	Ti ₂ O ₃	Mass Ratio
CS1	72.46	12.21	5.89	1.53	2.51	2.83	1.00	3.78	0.05
CS2	63.62	12.21	5.89	1.53	2.51	2.83	1.00	11.35	0.15
CS3	55.20	12.21	5.89	1.53	2.51	2.83	1.00	18.92	0.25
CS4	46.79	12.21	5.89	1.53	2.51	2.83	1.00	26.49	0.35
CS5	38.37	12.21	5.89	1.53	2.51	2.83	1.00	34.06	0.45
CS6	55.20	13.38	5.89	1.53	1.34	2.83	1.00	18.92	0.10
CS7	55.20	11.32	5.89	1.53	3.40	2.83	1.00	18.92	0.30
CS8	55.20	9.81	5.89	1.53	4.91	2.83	1.00	18.92	0.50
CS9	55.20	8.66	5.89	1.53	6.06	2.83	1.00	18.92	0.70
CS10	55.20	7.75	5.89	1.53	6.97	2.83	1.00	18.92	0.90

Figure 6 shows the effects of mass ratio of $\text{Ti}_2\text{O}_3/\Sigma\text{TiO}_2$ and the mass ratio of MgO/FeO on the total crystallization rates of anosovite crystals. It can be observed that the total crystallization rates of anosovite crystals increases one order of magnitude with the mass ratio of $\text{Ti}_2\text{O}_3/\Sigma\text{TiO}_2$ increasing from 0.05 to 0.45 and increases only three times with the mass ratio of MgO/FeO increasing from 0.10 to 0.90. It can be deduced that the mass ratio of $\text{Ti}_2\text{O}_3/\Sigma\text{TiO}_2$ has a remarkable influence on the total crystallization rate of anosovite crystals while the mass ratio of MgO/FeO has a slight influence on the total crystallization rate of anosovite crystals.

Figure 7 shows the effects of the mass ratio of $\text{Ti}_2\text{O}_3/\Sigma\text{TiO}_2$ and the mass ratio of MgO/FeO on the maximum total crystallization rate and peak temperature of anosovite crystals. It can be seen from Figure 7 that the maximum crystallization rate of anosovite crystals decreases with the mass ratio of $\text{Ti}_2\text{O}_3/\Sigma\text{TiO}_2$ increasing, while the maximum crystallization rate of anosovite crystals increases with the mass ratio of MgO/FeO increasing. This phenomenon can be attributed to the variation of the viscosity of titanium slag resulting from the composition change. The peak temperatures of total crystallization rates of anosovite crystals increase with the mass ratio of $\text{Ti}_2\text{O}_3/\Sigma\text{TiO}_2$ increasing, while the peak temperatures of total crystallization rates of anosovite crystals decrease with the mass ratio of MgO/FeO increasing. This phenomenon demonstrates that the increase in the viscosity of titanium slag leads to the diffusion difficulty of atoms and the larger degree of undercooling is needed to crystallize.

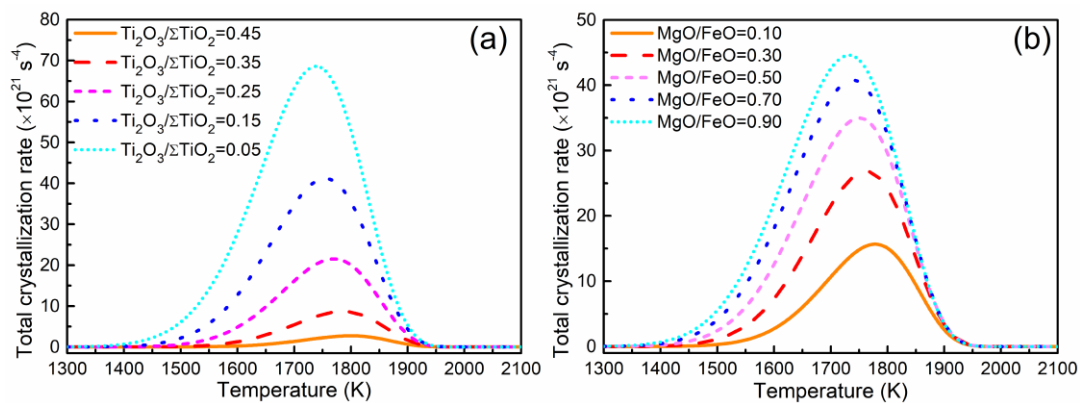


Figure 6. Effects of slag composition on total crystallization rates of anosovite crystals: (a) $\text{Ti}_2\text{O}_3/\Sigma\text{TiO}_2$ and (b) MgO/FeO .

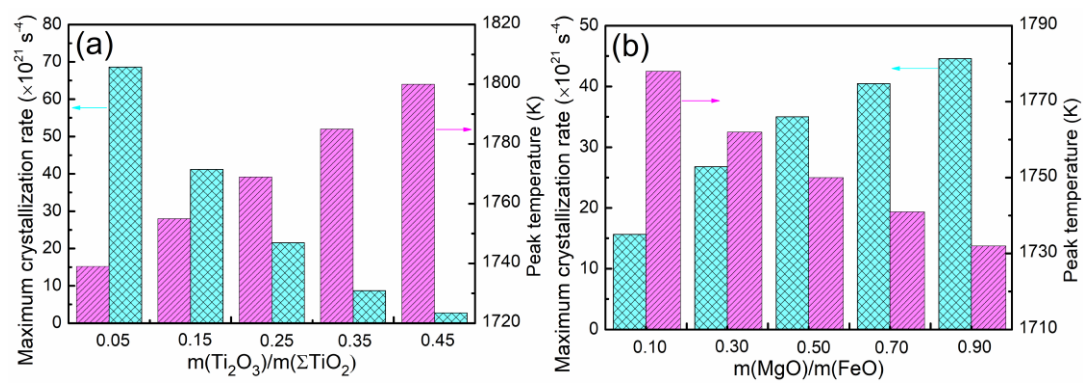


Figure 7. Effects of slag composition on maximum crystallization rates and peak temperatures of anosovite crystals: (a) $\text{Ti}_2\text{O}_3/\Sigma\text{TiO}_2$ and (b) MgO/FeO .

4. Conclusions

A mathematical model was established to describe the crystallization behaviors of anosovite and silicate crystals in high CaO and MgO titanium slag. The main results are shown as follows:

- (1) The crystallization order of anosovite and silicate crystals in high CaO and MgO titanium slag is obtained during cooling as follows: $\text{Al}_2\text{TiO}_5 > \text{Ti}_3\text{O}_5 > \text{MgTi}_2\text{O}_5 > \text{MgSiO}_3 > \text{CaSiO}_3 > \text{FeTi}_2\text{O}_5 > \text{Mn}_2\text{SiO}_4 > \text{Fe}_2\text{SiO}_4$.
- (2) The optimum temperature ranges of crystallization of these crystals in titanium slag are in their crystallization order as follows: 1744–1804 K, 1636–1696 K, 1589–1649 K, 1512–1572 K, 1502–1562 K, 1463–1523 K, 1346–1406 K, 1236–1296 K.
- (3) The total crystallization rates of anosovite and silicate crystals are mainly controlled by Al_2TiO_5 and MgSiO_3 , respectively. Al_2TiO_5 and Ti_3O_5 have a higher crystallization priority and should be responsible for the sharp increase in viscosity of titanium slag during cooling.
- (4) The mass ratio of $\text{Ti}_2\text{O}_3/\Sigma\text{TiO}_2$ has a remarkable influence on the total crystallization rate of anosovite crystals while the mass ratio of MgO/FeO has a slight influence on the total crystallization rate of anosovite crystals.

Author Contributions: H.F., D.C., T.L., and H.D. deduce and validate the model. H.F., T.L., Y.H., M.L. and W.H. performed the calculation. All of the authors analyzed and discussed the data; H.F. wrote the paper.

Funding: This research received no external funding.

Acknowledgments: Special appreciation is extended to PhD candidates Huabiao Chen and Sheng Yu at Chongqing University for the help on the graphic design.

Conflicts of Interest: The authors declare no conflict interest.

References

1. Liu, Y.; Meng, F.; Fang, F.; Wang, W.; Chu, J.; Qi, T. Preparation of rutile titanium dioxide pigment from low-grade titanium slag pretreated by the naoh molten salt method. *Dyes Pigment.* **2016**, *125*, 384–391.
2. Liu, W.; Lü, L.; Yue, H.; Liang, B.; Li, C. Combined production of synthetic rutile in the sulfate TiO₂ process. *J. Alloys Compd.* **2017**, *705*, 572–580. [[CrossRef](#)]
3. Fan, H.; Chen, D.; Liu, P.; Duan, H.; Huang, Y.; Long, M.; Liu, T. Structural and transport properties of feo-TiO₂ system through molecular dynamics simulations. *J. Non-Cryst. Solids* **2018**, *493*, 57–64. [[CrossRef](#)]
4. Cho, J.; Roy, S.; Sathyapalan, A.; Free, M.L.; Fang, Z.Z.; Zeng, W. Purification of reduced upgraded titania slag by iron removal using mild acids. *Hydrometallurgy* **2016**, *161*, 7–13. [[CrossRef](#)]
5. Chen, G.; Song, Z.; Chen, J.; Srinivasakannan, C.; Peng, J. Investigation on phase transformation of titania slag using microwave irradiation. *J. Alloys Compd.* **2013**, *579*, 612–616. [[CrossRef](#)]
6. Kondratiev, A.; Jak, E.; Hayes, P. Predicting slag viscosities in metallurgical systems. *JOM* **2002**, *54*, 41–45. [[CrossRef](#)]
7. Zhao, Z.; Ma, E.; Lian, Y. Behavior of Al₂O₃ in titanium slag. *Iron Steel Vanadium Titan.* **2002**, *23*, 36–38.
8. Li, S.; Lv, X.; Song, B.; Miu, H.; Han, K. Rheological property of TiO₂-FeO-(SiO₂, CaO, MgO) ternary slag. *Chin. J. Nonferrous Metals* **2016**, *26*, 2015–2022.
9. Handfield, G.; Charette, G. Viscosity and structure of industrial high TiO₂ slags. *Can. Metall. Q.* **1971**, *10*, 235–243. [[CrossRef](#)]
10. Gao, G.; Yang, Y.; Yang, D. Viscosity and melting point determination of titanium slag. *Iron Steel Vanadium Titan.* **1987**, *9*, 51–55.
11. Komatsu, T. Design and control of crystallization in oxide glasses. *J. Non-Cryst. Solids* **2015**, *428*, 156–175. [[CrossRef](#)]
12. Iqbal, N.; Van Dijk, N.; Offerman, S.; Moret, M.; Katgerman, L.; Kearley, G. Real-time observation of grain nucleation and growth during solidification of aluminium alloys. *Acta Mater.* **2005**, *53*, 2875–2880. [[CrossRef](#)]
13. Gan, L.; Zhang, C.; Shangguan, F.; Li, X. A differential scanning calorimetry method for construction of continuous cooling transformation diagram of blast furnace slag. *Metall. Mater. Trans. B* **2012**, *43*, 460–467. [[CrossRef](#)]
14. Gan, L.; Zhang, C.; Zhou, J.; Shangguan, F. Continuous cooling crystallization kinetics of a molten blast furnace slag. *J. Non-Cryst. Solids* **2012**, *358*, 20–24. [[CrossRef](#)]
15. Li, J.; Wang, X.; Zhang, Z. Crystallization behavior of rutile in the synthesized Ti-bearing blast furnace slag using single hot thermocouple technique. *ISIJ Int.* **2011**, *51*, 1396–1402. [[CrossRef](#)]
16. Klug, J.L.; Hagemann, R.; Heck, N.C.; Vilela, A.C.; Heller, H.P.; Scheller, P.R. Crystallization control in metallurgical slags using the single hot thermocouple technique. *Steel Res. Int.* **2013**, *84*, 344–351. [[CrossRef](#)]
17. Zhou, L.; Wang, W.; Huang, D.; Wei, J.; Li, J. In situ observation and investigation of mold flux crystallization by using double hot thermocouple technology. *Metall. Mater. Trans. B* **2012**, *43*, 925–936. [[CrossRef](#)]
18. Hu, M.; Liu, L.; Lv, X.; Bai, C.; Zhang, S. Crystallization behavior of perovskite in the synthesized high-titanium-bearing blast furnace slag using confocal scanning laser microscope. *Metall. Mater. Trans. B* **2014**, *45*, 76–85. [[CrossRef](#)]
19. Liu, J.; Verhaeghe, F.; Guo, M.; Blanpain, B.; Wollants, P. In situ observation of the dissolution of spherical alumina particles in CaO-Al₂O₃-SiO₂ melts. *J. Am. Ceram. Soc.* **2007**, *90*, 3818–3824.
20. Ruvalcaba, D.; Mathiesen, R.; Eskin, D.; Arnberg, L.; Katgerman, L. In situ observations of dendritic fragmentation due to local solute-enrichment during directional solidification of an aluminum alloy. *Acta Mater.* **2007**, *55*, 4287–4292. [[CrossRef](#)]
21. Watson, K.D.; Nguelo, S.T.; Desgranges, C.; Delhommelle, J. Crystal nucleation and growth in Pd-Ni alloys: A molecular simulation study. *CrystEngComm* **2011**, *13*, 1132–1140. [[CrossRef](#)]
22. Turnbull, D. Formation of crystal nuclei in liquid metals. *J. Appl. Phys.* **1950**, *21*, 1022–1028. [[CrossRef](#)]
23. Wu, F.; Li, X.; Wang, Z.; Wu, L.; Guo, H.; Xiong, X.; Zhang, X.; Wang, X. Hydrogen peroxide leaching of hydrolyzed titania residue prepared from mechanically activated panzhihua ilmenite leached by hydrochloric acid. *Int. J. Miner. Process.* **2011**, *98*, 106–112. [[CrossRef](#)]
24. Dong, H. Study on Production of High-Quality Synthetic Rutile from Electric Furnace Titanium Slag with High Content of Calcium and Magnesium. Ph.D., Thesis, Central South University, Changsha, China, 2010.

25. Fan, H.; Duan, H.; Tan, K.; Li, Y.; Chen, D.; Long, M.; Liu, T. Production of synthetic rutile from molten titanium slag with the addition of B₂O₃. *JOM* **2017**, *69*, 1914–1919. [[CrossRef](#)]
26. Seitz, F.; Turnbull, D. *Solid State Physics*; Academic Press: New York, NY, USA, 1958; Volume 7.
27. Meyer, R.E. Self-diffusion of liquid mercury. *J. Phys. Chem.* **1961**, *65*, 567–568. [[CrossRef](#)]
28. Hoffman, R.E. The self-diffusion of liquid mercury. *J. Chem. Phys.* **1952**, *20*, 1567–1570. [[CrossRef](#)]
29. Mills, K.C.; Sridhar, S. Viscosities of ironmaking and steelmaking slags. *Ironmak. Steelmak.* **1999**, *26*, 262–268. [[CrossRef](#)]
30. Zhang, Y. Electronegativities of elements in valence states and their applications. 1. Electronegativities of elements in valence states. *Inorg. Chem.* **1982**, *21*, 3886–3889.
31. Dimitrov, V.; Komatsu, T. Correlation among electronegativity, cation polarizability, optical basicity and single bond strength of simple oxides. *J. Solid State Chem.* **2012**, *196*, 574–578. [[CrossRef](#)]
32. Turnbull, D. Under what conditions can a glass be formed? *Contemp. Phys.* **2006**, *10*, 473–488. [[CrossRef](#)]
33. Uhlmann, D.R. A kinetic treatment of glass formation. *J. Non-Crystall. Solids* **1972**, *7*, 337–348. [[CrossRef](#)]
34. Dai, D. *Amorphous Physics*; Electronic Industry Press: Beijing, China, 1989.
35. Powder Diffraction File. *International Centre for Diffraction Data*; Swarthmore: Newtown Square, PA, USA, 2000.
36. Atlas, S. (Ed.) *By Vdeh*; Verlag Stahleisen GmbH: Düsseldorf, Germany, 1995; pp. 48–90.
37. Eriksson, G.; Pelton, A.D. Critical evaluation and optimization of the thermodynamic properties and phase diagrams of the MnO-TiO₂, MgO-TiO₂, FeO-TiO₂, Ti₂O₃-TiO₂, Na₂O-TiO₂, and K₂O-TiO₂ systems. *Metall. Mater. Trans. B* **1993**, *24*, 795–805. [[CrossRef](#)]
38. Song, B. *Rheological Property and Melt Structure of High Titania Slag*; Chongqing University: Chongqing, China, 2015.
39. Diao, J.; Zhou, W.; Gu, P.; Ke, Z.; Qiao, Y.; Xie, B. Competitive growth of crystals in vanadium–chromium slag. *CrystEngComm* **2016**, *18*, 6272–6281. [[CrossRef](#)]
40. Pistorius, P.C.; Kotzé, H. Role of silicate phases during comminution of titania slag. *Miner. Eng.* **2009**, *22*, 182–189. [[CrossRef](#)]
41. Wang, D.; Wang, Z.; Qi, T.; Wang, L.; Xue, T. Decomposition kinetics of titania slag in eutectic naoh-nano 3 system. *Metall. Mater. Trans. B* **2016**, *47*, 1–9.



© 2018 by the authors. Licensee MDPI, Basel, Switzerland. This article is an open access article distributed under the terms and conditions of the Creative Commons Attribution (CC BY) license (<http://creativecommons.org/licenses/by/4.0/>).